

Study of Surface and Bulk Acoustic Phonon Excitations in Superlattices using Picosecond Ultrasonics

Nen-Wen Pu

Department of Applied Physics, Chung Cheng Institute of Technology, National Defense University, Tahsi, Taoyuan 335, Taiwan

Jeffrey Bokor

Department of Electrical Engineering and Computer Science, University of California, Berkeley, California 94720-1772, USA
(Received 9 May 2003; published 11 August 2003)

We have performed picosecond ultrasonic studies on the surface and bulk acoustic phonons in amorphous Mo/Si superlattices. Localized surface modes within the first, second, and sixth frequency gaps of the zone-folded phonons are observed. A selection rule derived from symmetry considerations provides new understanding of why certain modes are seen and not the others. The excitation strengths and detailed spectral features of these lines are studied, and the results are well explained by an elastic-continuum theory. It is found that the line shapes are significantly modified by the presence of bulk modes near the zone center.

DOI: 10.1103/PhysRevLett.91.076101

PACS numbers: 68.65.Cd, 63.20.-e, 78.47.+p

In a superlattice the artificial periodicity along the direction perpendicular to the layers leads to profound modifications in the propagation of acoustic phonons. The phonon dispersion curve is backfolded into a series of minibranches and gaps open at the boundaries and the center of the mini-Brillouin zone [1,2] of dimension $2\pi/d$, where d is the modulation period. Evidence for the folding is found in low-frequency Raman spectra [1,3], which show doublets of longitudinal acoustic (LA) phonons with a fixed transfer of crystal momentum. No propagating modes are allowed within the gaps, where the wave number q becomes complex, but in semi-infinite structures there remains the possibility of exciting non-propagating evanescent modes localized near the free surface [4,5]. These modes have been experimentally observed by time-resolved picosecond laser ultrasonics [6–13] and Raman spectra [3], separately. However, what remains unsolved is that, although surface modes are expected to exist within each gap on the folded LA dispersion curve (exactly one per gap) according to the theory, modes higher than the second gap have never been observed experimentally.

In this Letter we report on the first observation of the surface mode within the sixth gap in a series of amorphous Mo/Si superlattices. This sixth-gap mode diminishes much faster than the lower-gap modes as d decreases, and could not be detected in the superlattices with the shortest period. A selection rule based on symmetry considerations of the laser-induced stress and the surface-mode waveforms is proposed to explain why only the modes within the first, second, and sixth gaps are seen and not the others. In addition, we have investigated the simultaneous excitations of these surface modes together with the folded LA phonons (bulk modes) by ultrashort light pulses. The presence of bulk modes modifies the line shapes significantly.

Phonons are impulsively excited in superlattices by an ultrashort “pump” light pulse (energy ~ 0.3 nJ), and detected as a reflectivity change of a weaker (~ 0.03 nJ), time-delayed “probe” pulse. The output of a mode-locked Ti:sapphire laser operating at 800 nm, with a full width at half maximum (FWHM) pulse duration of 190 fs is split to obtain these pulses. The details of the optical arrangement were described in our previous works [11,13]. A slight change ($\sim 0.001\%$) of the optical reflectivity $\Delta R(t)$ is induced by the acoustic waves through photoelastic effect. Figure 1(a) displays the measured $\Delta R(t)$ traces for samples with various d : 326, 196, and 68.4 Å (a smoothly varying background has been subtracted out). The number of periods is 40 and the relative Mo thickness ratio Γ ($\equiv d_{\text{Mo}}/d$) is 0.5. The beating seen in the traces indicates simultaneous excitations of at least two surface modes. The frequencies ν_{sn} (n is the

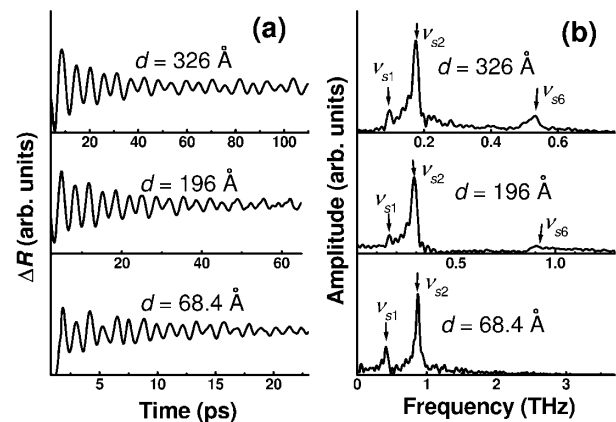


FIG. 1. (a) The measured $\Delta R(t)$ for Mo/Si superlattices with $d = 326$, 196, and 68.4 Å ($\Gamma = 0.5$). A smoothly varying background has been subtracted out. (b) The corresponding Fourier transform spectra.

index for gaps or surface modes) of these modes are solutions of [6]

$$\tan\left(\frac{2\pi\nu_{sn}d_2}{c_2}\right) + \frac{\rho_1 c_1}{\rho_2 c_2} \tan\left(\frac{2\pi\nu_{sn}d_1}{c_1}\right) = 0, \quad (1)$$

where d_i , ρ_i , and c_i are the thicknesses, densities, and sound velocities of the constituents ($i = 1$ for Si; 2 for Mo). Figure 1(b) shows the corresponding vibration spectra. In all of the samples, we observe the surface modes in the first (lowest zone edge) gap and the second (lowest zone center) gap. In addition to these two modes, a higher-order surface mode is also seen in samples with $d = 326$ and 196 \AA . The amplitude of this mode decreases rapidly as d is reduced from 326 to 196 \AA , and vanishes in the thinnest sample ($d = 68.4 \text{ \AA}$). Theoretical calculation indicates that it is the surface mode in the sixth (third zone center) gap. The theoretical and measured values of the surface-mode frequencies ν_{s1} , ν_{s2} , and ν_{s6} are listed in Table I. Although the measured frequencies are somewhat lower than the theoretical values (by $<16\%$), they do follow a linear relation with $1/d$ in accordance with Eq. (1). This frequency mismatch might be caused by silicide (a few angstroms thick) formation at Mo/Si interfaces [14], or modified elastic properties in thin films [15].

The trend that higher-gap modes diminish faster as d decreases can be understood from the microscopic dynamics of acoustic wave generation. The optical energy is predominantly absorbed by the electrons in Mo. These hot electrons take a few hundred femtoseconds to thermalize with lattice via electron-phonon (e - p) interaction [16], so the coherent generation of high-frequency lattice vibrations ($> 1 \text{ THz}$) will be greatly suppressed. To explain why certain modes are selectively excited and how their relative strengths vary, we performed numerical simulations for acoustic wave generation and evolution in superlattices. The spatiotemporal profile of the strain wave $\eta(z, t)$ is obtained by solving the 1D equations of elasticity within each layer [17]:

$$\sigma(z, t) = 3\left(\frac{1-\mu}{1+\mu}\right)B\eta(z, t) - 3B\beta\Delta T(z, t) \quad (2)$$

and

TABLE I. Frequencies of the surface modes in the first, second, and sixth gaps determined from theory ($\nu_{s1 \text{ th}}$, $\nu_{s2 \text{ th}}$, and $\nu_{s6 \text{ th}}$) and experiment ($\nu_{s1 \text{ exp}}$, $\nu_{s2 \text{ exp}}$, and $\nu_{s6 \text{ exp}}$).

d (\AA)	$\nu_{s1 \text{ th}}$ (GHz)	$\nu_{s2 \text{ th}}$ (GHz)	$\nu_{s6 \text{ th}}$ (GHz)	$\nu_{s1 \text{ exp}}$ (GHz)	$\nu_{s2 \text{ exp}}$ (GHz)	$\nu_{s6 \text{ exp}}$ (GHz)
326	103	194	584	94	179	532
196	172	323	972	158	298	904
68.4	491	923	2780	413	873	...

$$\rho \frac{\partial^2 u(z, t)}{\partial t^2} = \frac{\partial \sigma(z, t)}{\partial z}, \quad (3)$$

where σ is the zz component of stress, u is the displacement in the z direction ($\frac{\partial u}{\partial z} = \eta$), ΔT is the rise in lattice temperature, β is the thermal expansion coefficient, B is the bulk modulus, and μ is the Poisson's ratio. The boundary conditions require that σ be zero at the free surface $z = 0$, and that both σ and u be continuous at the interfaces. For simplicity, the contribution to stress field from hot electrons is ignored. The last term in Eq. (2) corresponds to a time-varying thermal stress due to lattice expansion and acts as a continuous driving force for elastic waves. A complete simulation should incorporate the equation of heat diffusion to calculate the evolution of lattice temperature $T(z, t)$:

$$\frac{\partial^2 T}{\partial z^2} + S(z, t) = \frac{1}{D} \frac{\partial T}{\partial t}, \quad (4)$$

where D is the thermal diffusivity and $S(z, t)$ is the heat source. Finally, the photoelastic response $\Delta R(t)$ is related to the strain wave $\eta(z, t)$ through a depth-dependent "sensitivity function" $f(z)$ [6,7,17]:

$$\Delta R(t) = \int_0^\infty f(z)\eta(z, t)dz.$$

A way to simplify the calculation is to assume that the light pulse sets up an initial stress $\sigma(z, 0)$ *instantaneously* [6], that is, we neglect the last term in Eq. (2), and solve the *undriven* wave equation. The calculated vibrations are undamped due to the lack of loss mechanism in our equations, so we enforce a damping time constant τ to obtain a line width that agrees best with experiments. Figure 2(a) shows the calculated spectrum for $d = 70 \text{ \AA}$ and $\Gamma = 0.5(\tau = 15 \text{ ps})$. The two lines at 0.90 and 2.71 THz correspond to the surface modes ν_{s2} and ν_{s6} , respectively. Their frequencies agree with the theoretical values predicted by Eq. (1). However, the relative excitation strengths are by no means close to the experiment.

To acquire a correct spectrum, we need to consider the finite buildup time for the thermal stress term. The heat source in Eq. (4) is assumed to be a Gaussian pulse in time:

$$S(z, t) = \frac{W(z)}{k} \frac{1}{t_1 \sqrt{\pi}} e^{-t^2/t_1^2},$$

where $W(z)$ is the optically deposited energy density, k is the thermal conductivity, and the adjustable variable t_1 takes into account both the finite laser pulse width and the delay due to e - p heat exchange. The calculated spatial form of $W(z)$ is a square wave ($= 1$ in Mo; ~ 0 in Si) decaying exponentially with an effective skin depth of ζ/Γ , where ζ is the optical skin depth of Mo. Figure 2(b) shows the result for $t_1 = 228 \text{ fs}$, which corresponds to a 190 fs FWHM laser pulse width (i.e., without broadening

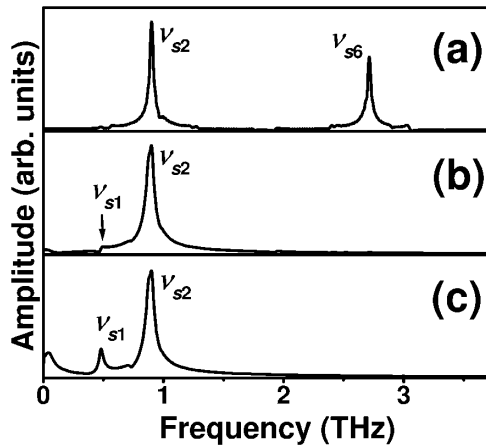


FIG. 2. The calculated vibration spectra for $d = 70 \text{ \AA}$ and $\Gamma = 0.5$: (a) assuming *instantaneous* buildup of lattice stress; (b) considering a finite buildup time $t_1 = 228 \text{ fs}$ (laser pulse width); (c) using a longer buildup delay $t_1 = 600 \text{ fs}$.

from e - p interaction). The sixth-gap mode already disappears completely. The second-gap mode is slightly suppressed but still overestimated. The best spectrum is obtained for $t_1 \sim 600 \text{ fs}$ [see Fig. 2(c)], which is 3 times longer than the laser pulse width, indicating a substantial delay for the energy transfer from electrons to lattice. The vibration spectrum is nicely reproduced except for low-frequency components, which are considerably smaller in the measured spectrum owing to the cancellation effect of our alternating-pump technique[11]. The calculated relative intensity of the lines ν_{s1} and ν_{s2} varies rapidly (in a time scale of 100 fs) with t_1 . We believe that it provides a sensitive way to estimate the e - p coupling constant g (see Ref. [16]) in metals.

The reason why only the surface modes $n = 1, 2$, and 6 can be excited in superlattices is as follows: The stress pattern and the sensitivity function both have the periodicity of the superlattice [8]. They couple poorly to all zone-boundary surface modes ($n = 1, 3, 5, \dots$) whose waveforms $[\eta(z)]$ invert from one period to the next, and to the even zone-center modes ($n = 4, 8, 12, \dots$), which are approximately antisymmetric within each sublayer. Therefore only the *odd zone-center* surface modes ($n = 2, 6, 10, \dots$) are strongly excited and detected. However, the coupling coefficient is roughly proportional to $(1/n)$, so the modes higher than $n = 6$ have less chance to be observed. The n -selection rule is relaxed for the ν_{s1} line owing to its short decay length. In addition, the damping rate of this mode is the lowest among all surface modes, and so it is easier to be detected.

The shape of the ν_{s2} line shows interesting dependence on Γ . Spectra measured in samples with $d = 69.0 \text{ \AA}$ and Γ varying from 0.3 to 0.6 are displayed in Fig. 3. For $\Gamma = 0.5$ and 0.6, the ν_{s2} line has an asymmetric shape with a tail toward low frequencies. In the spectra for $\Gamma = 0.3$ and 0.4, this line is clearly broadened and the line shape

becomes much more complicated. To understand the origin of these strange line shapes we performed the calculations mentioned above, and the results are shown in Fig. 4. Except for $\Gamma = 0.4$, all measured spectra are satisfyingly reproduced. The experimentally observed line shape for $\Gamma = 0.4$ (Fig. 3)—featuring double peaks with a sharp dip in between—is found instead in the calculated spectrum labeled $\Gamma = 0.37$ ($d_{\text{Mo}} = 26 \text{ \AA}$). This minor disagreement can be explained by the effect of silicide formation [14], which makes the real thickness of Mo a few angstroms less than the as-deposited value.

The side peaks and the asymmetric line shapes are associated with the bulk modes near the upper (ν_{2+}) or lower (ν_{2-}) edges of the second frequency gap (see the upper part of Fig. 4 and also the vertical lines in the spectra). These modes are strongly excited due to the high density of states and continuously detected due to the low group velocity to move away from surface. To justify this assignment, we first calculated the spectra for superlattices terminated by a Mo surface layer. All surface modes vanish as expected [6], but the peaks near ν_{2+} or ν_{2-} are still present. Next, we try to separate the surface-part contribution to ΔR from the bulk contribution. The dashed curves and the dotted curves in Fig. 4 are obtained by letting $f(z)$ be zero for $z > 250 \text{ \AA}$ or for $z < 250 \text{ \AA}$, respectively. Evidently the higher-frequency peak in the spectra for $\Gamma = 0.37$ and 0.3 is due to the ν_{2+} bulk modes, which extend throughout the superlattice, and the lower-frequency peak is the zone-center surface mode ν_{s2} , which has an attenuation length of tens or hundreds of angstroms. For $\Gamma = 0.3$, the ν_{2+} bulk modes are even more intensely excited than the surface mode. In the spectra for $\Gamma = 0.5$ and above, the ν_{2-} bulk modes, instead of ν_{2+} , are observed and cause the asymmetrization of the line shape. For any Γ , only one of the ν_{2+} and

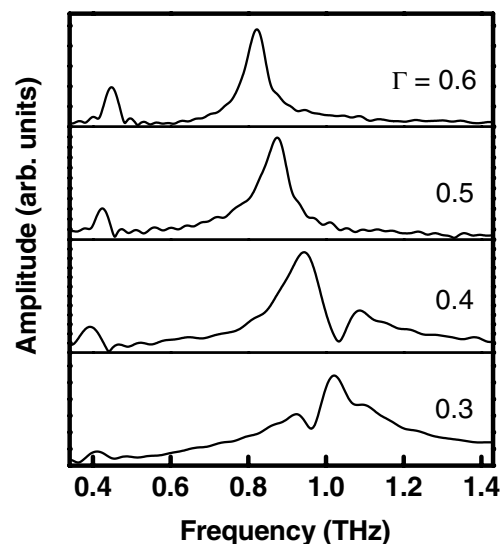


FIG. 3. Comparison of the observed vibration spectra for $\Gamma = 0.6, 0.5, 0.4$, and 0.3 ($d = 69 \text{ \AA}$).

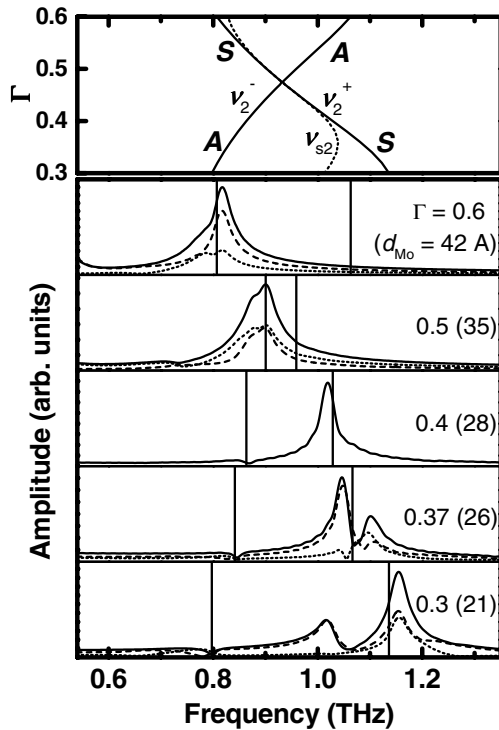


FIG. 4. The calculated spectra for $\Gamma = 0.6, 0.5, 0.4, 0.37,$ and 0.3 ($d = 70 \text{ \AA}$). The vertical lines define the upper (ν_{2+}) and lower (ν_{2-}) edges of the second gap. The dashed curves and the dotted curves are obtained by letting $f(z)$ be zero for $z > 250 \text{ \AA}$ or for $z < 250 \text{ \AA}$, respectively. The upper part of the figure shows the theoretical values of ν_{s2} (dotted curves), ν_{2-} , and ν_{2+} vs Γ . The symmetry of the bulk modes at the gap edges is indicated with S (symmetric) or A (antisymmetric). Note the crossover at $\Gamma = 0.474$.

ν_{2-} peaks is strongly excited. To explain this observation, we indicate the symmetry for ν_{2+} and ν_{2-} modes in the upper part of Fig. 4: S for symmetric and A for antisymmetric strain fields $[\eta(z)]$ within each sublayer. The A waves cannot be detected because they couple poorly to the sensitivity function $f(z)$, which is approximately symmetric within each sublayer when d is much shorter than the wavelength of light in the material (see Ref. [17]). The S waves, which are optically detectable, lie at the upper edge of the second gap (ν_{2+}) for small Γ , and cross over to the lower edge (ν_{2-}) for $\Gamma > 0.474$. Consequently, the ν_{2+} and ν_{2-} peaks emerge correspondingly for Γ below or above this crossover point.

In summary, we have studied the excitations of LA surface and bulk phonons in a series of Mo/Si superlattices. As many as three surface modes ($n = 1, 2,$ and 6) are observed. A selection rule derived from symmetry considerations is proposed to explain why only these modes are excited. The sixth-gap mode diminishes rapidly when its frequency reaches 1 THz due to the finite delay time for e - p interaction. Besides the surface modes, bulk modes near the second gap are also excited and

result in complicated line shapes. The special features of the vibration spectra are nicely reproduced by theoretical calculations.

This work was supported in part by the National Science Council of Taiwan under Grant No. NSC 91-2112-M-014-001, Semiconductor Research Corporation under Contract No. 96-LC-460, and DARPA Advanced Lithography Program under Grant No. MDA972-97-0010.

- [1] C. Colvard, R. Merlin, M.V. Klein, and A.C. Gossard, *Phys. Rev. Lett.* **45**, 298 (1980).
- [2] B. Jusserand and M. Cardona, in *Light Scattering in Solids V: Superlattices and Other Microstructures*, edited by M. Cardona and G. Guntherodt, Topics in Applied Physics Vol. 66 (Springer-Verlag, Berlin, 1989).
- [3] H.J. Trodahl, P.V. Santos, G.V.M. Williams, and A. Bittar, *Phys. Rev. B* **40**, 8577 (1989).
- [4] R.E. Camley, B. Djafari-Rouhani, L. Dobrzynski, and A.A. Maradudin, *Phys. Rev. B* **27**, 7318 (1983).
- [5] B. Djafari-Rouhani, L. Dobrzynski, O. Hardouin Duparc, R.E. Camley, and A.A. Maradudin, *Phys. Rev. B* **28**, 1711 (1983).
- [6] H.T. Grahn, H.J. Maris, J. Tauc, and B. Abeles, *Phys. Rev. B* **38**, 6066 (1988).
- [7] H.T. Grahn, H.J. Maris, and J. Tauc, *IEEE J. Quantum Electron.* **25**, 2562 (1989).
- [8] W. Chen, Y. Lu, H.J. Maris, and G. Xiao, *Phys. Rev. B* **50**, 14506 (1994).
- [9] B. Perrin, B. Bonello, J.C. Jeannet, and E. Romatet, *Physica (Amsterdam)* **219B&220B**, 681 (1996).
- [10] B. Bonello, B. Perrin, E. Romatet, and J.C. Jeannet, *Ultrasonics* **35**, 223 (1997).
- [11] N-W. Pu, S. Jeong, R-A. Zhao, and J. Bokor, *Appl. Phys. Lett.* **74**, 320 (1999).
- [12] N-W. Pu, S. Jeong, R-A. Zhao, and J. Bokor, in *Proceedings of SPIE on Emerging Lithographic Technologies III*, SPIE Proceedings Vol. 3676 (SPIE-International Society for Optical Engineering, Bellingham, WA, 1999), p 627.
- [13] N-W. Pu, J. Bokor, S. Jeong, and R-A. Zhao, *J. Vac. Sci. Technol. B* **17**, 3014 (1999).
- [14] R.S. Rosen, D.G. Stearns, M.A. Viliardos, M.E. Kassner, S.P. Vernon, and Y. Cheng, *Appl. Opt.* **32**, 6975 (1993).
- [15] B.M. Clemens and G.L. Eesley, *Phys. Rev. Lett.* **61**, 2356 (1988); E.E. Fullerton, I.K. Schuller, F.T. Parker, K.A. Svinarich, G.L. Eesley, R. Bhadra, and M. Grimsditch, *J. Appl. Phys.* **73**, 7370 (1993). For the moment, we take the values for bulk, crystalline Si and Mo: $\rho_{\text{Si}} = 2.33 \text{ g/cm}^3$, $c_{\text{Si}} = 6.9 \times 10^5 \text{ cm/s}$, $\rho_{\text{Mo}} = 10.22 \text{ g/cm}^3$, and $c_{\text{Mo}} = 6.2 \times 10^5 \text{ cm/s}$.
- [16] S.I. Anisimov, B.L. Kapeliovich, and T.L. Perel'man, *Zh. Eksp. Teor. Fiz.* **66**, 776 (1974) [*Sov. Phys. JETP*, **39**, 375 (1975)]; J.G. Fujimoto, J.M. Liu, E.P. Ippen, and N. Bloembergen, *Phys. Rev. Lett.* **53**, 1837 (1984); R.W. Schoenlein, W.Z. Lin, J.G. Fujimoto, and G.L. Eesley, *Phys. Rev. Lett.* **58**, 1680 (1987).
- [17] C. Thomsen, H.T. Grahn, H.J. Maris, and J. Tauc, *Phys. Rev. B* **34**, 4129 (1986).